EUROfusion

EUROFUSION CP(15)03/15

M.J. Mantsinen et al.

# Bulk Ion Heating with ICRF Waves in Tokamaks

(27th April 2015 – 29th April 2015)
Lake Arrowhead, California, USA

This work has been carried out within the framework of the EUROfusion Consortium and has received funding from the Euratom research and training programme 2014-2018 under grant agreement No 633053. The views and opinions expressed herein do not necessarily reflect those of the European Commission.

# Bulk Ion Heating with ICRF Waves in Tokamaks

M.J. Mantsinen[1,2,a)], R. Bilato[3], V.V. Bobkov[3], A. Kappatou[3], R. M. McDermott[3], M. Nocente[4,5], T. Odstrčil[3], G.Tardini[3], M. Bernert[3], R. Dux[3], T. Hellsten[6], P. Mantica[5], M. Maraschek[3], S.K. Nielsen[7], J-M. Noterdaeme[3], J. Rasmussen[7], F. Ryter[3], M. Stejner[7], J. Stober[3], M. Tardocchi[5] and the ASDEX Upgrade Team and the EUROfusion MST1 Team

[1]*Catalan Institution for Research and Advanced Studies, Barcelona, Spain*
[2]*Barcelona Supercomputing Center, Barcelona, Spain*
[3]*Max-Planck-Institut für Plasmaphysik, Garching, Germany*
[4]*Dipartimento di Fisica "G. Occhialini", Università degli Studi di Milano-Bicocca, Milano, Italy*
[5]*Istituto di Fisica del Plasma "P. Caldirola", CNR, Milano, Italy*
[6]*Dept. of Fusion Plasma Physics, EES, KTH, Stockholm, Sweden*
[7]*Technical University of Denmark, Department of Physics, Lyngby, Denmark*
[a)]*Corresponding author: mervi.mantsinen@bsc.es*

**Abstract.** Heating with ICRF waves is a well-established method on present-day tokamaks and one of the heating systems foreseen for ITER. However, further work is still needed to test and optimize its performance in fusion devices with metallic high-Z plasma facing components (PFCs) in preparation of ITER and DEMO operation. This is of particular importance for the bulk ion heating capabilities of ICRF waves. Efficient bulk ion heating with the standard ITER ICRF scheme, i.e. the second harmonic heating of tritium with or without $^3$He minority, was demonstrated in experiments carried out in deuterium-tritium plasmas on JET and TFTR and is confirmed by ICRF modelling. This paper focuses on recent experiments with $^3$He minority heating for bulk ion heating on the ASDEX Upgrade (AUG) tokamak with ITER-relevant all-tungsten PFCs. An increase of 80% in the central ion temperature $T_i$ from 3 to 5.5 keV was achieved when 3 MW of ICRF power tuned to the central $^3$He ion cyclotron resonance was added to 4.5 MW of deuterium NBI. The radial gradient of the $T_i$ profile reached locally values up to about 50 keV/m and the normalized logarithmic ion temperature gradients $R/L_{Ti}$ of about 20, which are unusually large for AUG plasmas. The large changes in the $T_i$ profiles were accompanied by significant changes in measured plasma toroidal rotation, plasma impurity profiles and MHD activity, which indicate concomitant changes in plasma properties with the application of ICRF waves. When the $^3$He concentration was increased above the optimum range for bulk ion heating, a weaker peaking of the ion temperature profile was observed, in line with theoretical expectations.

## INTRODUCTION

Heating with waves in the ion cyclotron range of frequencies (ICRF) is a well-established method and plays a key role in the operation and plasma performance optimization in several present-day fusion devices. However, further research is still needed in its use in fusion devices with metallic high-Z plasma facing components in preparation of ITER operation. In ITER, ICRF waves will be used for heating ITER plasmas to thermonuclear temperatures. In this task, heating fuel ions will be of particular importance. Not only is it necessary to achieve the target fusion yield but also to ensure control during the ramp-up phase and to ease the access to the H-mode with improved confinement. Among the auxiliary heating schemes envisaged for ITER, ICRF heating is the only scheme that can provide dominant bulk ion heating. The other heating methods, the electron cyclotron waves and neutral beam injection of MeV-energy-range ions, will provide mainly electron heating.

Bulk ion heating with ICRF waves is achieved through the absorption of the wave power by resonant ions which collisionally transfer their energy to the fuel ions. This gives rise to two main conditions that need to be satisfied in

order to achieve bulk ion heating with ICRF waves. Firstly, the fraction of the ICRF power going to ion cyclotron damping needs to be significant with respect to other damping mechanisms. As a result of ion cyclotron damping, a high-energy tail often develops in the distribution function of the resonant ions. Secondly, this ICRF-accelerated fast ion tail needs to be tailored so that the energy of the fast ions remains below or close to the critical energy

$$E_{crit} \approx 14.8\, A T_e \left( \sum_j \frac{n_j Z_j^2}{n_e A_j} \right)^{2/3}$$

at which they transfer energy equally to electrons and ions in collisions. Here, *A* is the fast ion mass number, $T_e$ and $n_e$ are the electron temperature and density, respectively, and the sum goes over the ion species, with $A_j$, $Z_j$ and $n_j$ being the mass number, charge number and density of the ion species j. For standard ICRF minority heating schemes, the above conditions are satisfied within a range of optimal minority ion concentrations for which bulk ion heating is maximized. At lower concentrations, the fast ion tail tends to be too energetic for efficient bulk ion heating. At higher concentrations, ICRF mode conversion, which typically results in electron heating, starts to become important.

For ITER the standard ICRF scenario is the second harmonic heating of tritium. Given that $E_{crit}$ = 600 keV for tritium in ITER D-T plasma at a nominal $T_e$ of 25 keV, this scheme is compatible with bulk ion heating. Furthermore, since the second harmonic ion cyclotron frequency of tritium coincides with the fundamental ion cyclotron frequency of $^3$He, using small amounts of $^3$He minority ions in the plasma provides a means to optimize the performance characteristics of the scenario. This may become relevant e.g. in the plasma ramp up phase when the fast tritium tail ions may become too energetic for efficient bulk ion heating [1-3]. The bulk ion heating capabilities of the $\omega = \omega(^3\text{He}) = 2\,\omega_T$ scenario were successfully demonstrated in the 1990's in the flagship deuterium-tritium (D-T) campaigns in TFTR [4,5] and in JET [6-12]. Subsequently, $^3$He minority heating has become a standard tool on JET to provide bulk ion heating without net toroidal torque for ITER physics studies, c.f. for example [13,14]. It has also been successfully tested on other tokamaks [15-17]. In this paper we report on recent experiments to establish $^3$He minority heating as a scheme to heat bulk ions on the ASDEX Upgrade (AUG) tokamak which is a middle-sized divertor tokamak (R = 1.65 m, a = 0.5 m) with ITER-relevant all-tungsten plasma facing components.

## EXPERIMENTAL SET-UP

The experiments were carried out on in AUG H-mode deuterium plasmas in a single-null divertor configuration at a magnetic field of 2.8 and 3 T. Up to 3.5 MW of ICRF power was applied at a frequency of 30 MHz, which placed the $^3$He minority resonance in the plasma centre at a major radius of $R_{res} \approx 1.55$ m and 1.65 m (corresponding to $x/a \approx -0.3$ and -0.1) for 2.8 T and 3T, respectively. Here, $x = R_{res} - R_0$ and $R_0$ is the major radius at the magnetic axis. ICRF power was modulated at 4 and 8 Hz to study the plasma response. The $0\pi$ phasing of the ICRF antennas was used without applying net toroidal torque to the plasma. Operation at a low plasma current of 0.6 MA ($q_{95} \approx$ 8-8.5) was chosen as a preventive measure against impurity accumulation. However, impurity accumulation was not completely avoided in these experiments as will be shown later. In addition of ICRF heating, 4.5-6.5 MW of deuterium NBI was applied for plasma preheating and diagnostic purposes. For comparisons with ICRF power modulation, discharges with NBI modulation were also performed.

The $^3$He concentration with respect to $n_e$, resulting from the application of $^3$He puff from a gas valve at the mid plane, was deduced from charge exchange recombination spectroscopy (CXSR) taking into account the He "plume" effect [18]. The $^3$He concentration was varied between 1-12%. Figure 1 shows the time evolution of the measured total helium ($^3$He and $^4$He) concentration and the estimated $^3$He concentration at the mid radius for discharge 31555. In discharge 31555 three $^3$He puffs were applied at t = 1.2 s, 2.2 s and 3.2 s with a duration of 100 ms which are also shown in Fig. 1. The $^3$He concentration was estimated from the measured total helium ($^3$He and $^4$He) concentration assuming that the $^4$He concentration is equal to the measured He concentration of 1.5 % at the beginning of discharge 31552 before $^3$He was puffed into the machine. As we can see from Fig. 1, the $^3$He concentration increases rapidly after each $^3$He puff and then decays. The $^3$He concentration varied 2% and 4.5% in the time interval from t = 1.3 s to t = 4.5 s prepared for ICRF heating. In later discharges, a series of smaller and more frequent $^3$He puffs were successfully employed to keep the $^3$He concentration constant during the ICRF phase.

In addition to providing information on the $^3$He concentration, CXRS was used to measure the ion temperature $T_i$ and toroidal rotation. Fast Fourier analysis techniques were applied to study the $T_i$ response with respect to the applied ICRF power modulation. $T_e$ was measured with Thomson scattering diagnostics. However, its time

resolution was not high enough to allow the study of the $T_e$ response using fast Fourier analysis. $T_e$ was also measured by electron cyclotron emission spectroscopy but its radial range covered only the outer part of the plasma up to the mid radius given the range of magnetic fields (2.8-3T) used in these experiments.

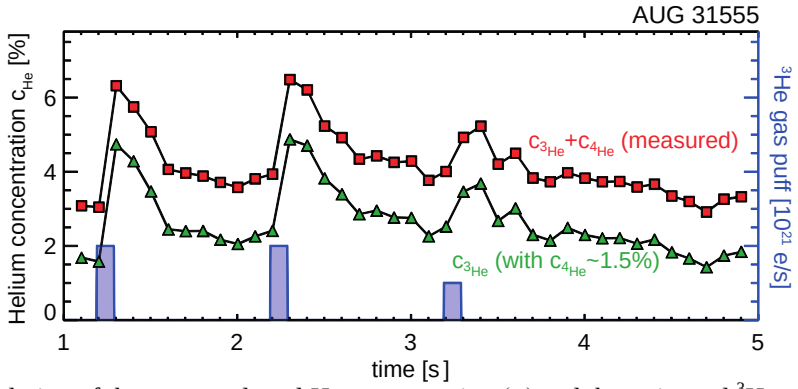


**FIGURE 1** Time evolution of the measured total He concentration (□) and the estimated $^3$He concentration (Δ) with respect to $n_e$ in discharge 31555. Also shown are the $^3$He puffs applied at t = 1.2 s, 2.2 s and 3.2 s.

## RESULTS

Figure 2 shows an overview of the main plasma parameters for 0.6 MA/ 3 T AUG discharge 31563 with ICRF heating tuned to a central $^3$He resonance at $R_{res}$≈1.65 m (x/a ≈ -0.1). For comparison, the parameters are also shown for 0.6 MA / 2.8 T discharge 31555 prepared in the same way but without ICRF heating. The evolution of the $^3$He concentration in discharge 31563 was similar to that in 31555 (cf. Fig. 1) and varied between 1.5 and 6% during the ICRF heating phase. As we can see from Fig. 2, with the application of 3.5 MW of ICRF power to 4.5 MW of deuterium NBI in discharge 31563, about 80% higher $T_i$ was obtained than in discharge 31555 with NBI only. In addition to the $T_i$ increase, $T_e$ as measured by Thomson scattering at R = 1.8 m (x/a ≈ 0.2) increased from about 2.5 keV in discharge 31555 to about 3 keV in discharge 31563. An increase in the plasma energy content is also observed. The H mode factor with respect to the H98(y,2) scaling was 0.8-0.85 and the normalized plasma beta $\beta_N$ was 1.0-1.15.

The radial profile of the amplitude and phase of the $T_i$ modulation as deduced from CXRS with respect to the applied ICRF power modulation in discharge 31563 is shown in Figure 3. The $T_i$ modulation amplitude reaches its maximum value of about 400 eV, and the phase of $T_i$ modulation its minimum value, around the ICRF resonance, which is consistent with the expected location of bulk ion heating due to $^3$He minority heating in this discharge.

The radial $T_i$ profiles for discharges 31555 and 31563 with NBI and on-axis ICRF are shown in Fig. 4 together with the radial $T_e$ profiles. The profiles are taken at t = 3 s towards the end of the phase with the maximum power in the ICRF power modulation cycle in discharge 31563. For comparison, we also show the $T_i$ and $T_e$ profiles for discharge 31562 which was prepared in the same way as discharge 31563 apart from the magnitude of the magnetic field. In discharge 31562 the magnetic field was 2.8 T which places the $^3$He resonance off-axis on the high field side at $R_{res}$≈1.55 m (x/a ≈ -0.3). As we can see from Fig. 4, the radial $T_i$ profiles for discharges 31562 and 31563 with $^3$He minority heating are significantly more peaked in the plasma center than the $T_i$ profile for discharge 31555 with NBI only. With the central ICRF resonance in discharge 31563, stronger $T_i$ peaking is obtained than with the off-axis resonance in discharge 31562. The $T_i$ profiles for discharge 31563 are characterized by radial gradients of ~50 keV/m and normalized logarithmic ion temperature gradient lenghts of $R/L_{Ti}$ of ~20, which are unusually large for AUG plasmas. As we can see from Fig. 4, no major differences are observed in the measured radial $T_e$ profile shapes between the three discharges. The electron density profiles, as shown in Fig. 5a, were relatively flat and identical within the error bars (not shown).

Apart from the differences in $T_i$, $T_e$ and plasma energy content in discharges 31555, 31562 and 31563, important further differences were observed in the plasma toroidal rotation, plasma impurity content and MHD activity which have important consequences for the understanding of the experimental results and for the assessment of the actual bulk ion heating achieved with ICRF waves in these discharges. We will discuss next these experimentally observed differences, followed by a brief discussion.

Figure 5b shows the plasma toroidal rotation velocity profiles as measured with CXSR at t = 3.1s for the three discharges. The toroidal rotation velocity increases when $^3$He minority heating is added to NBI even though no net torque is applied by ICRF waves. Furthermore, off-axis ICRF heating resulted in a broader toroidal rotation velocity with higher velocities in the plasma center than central ICRF.

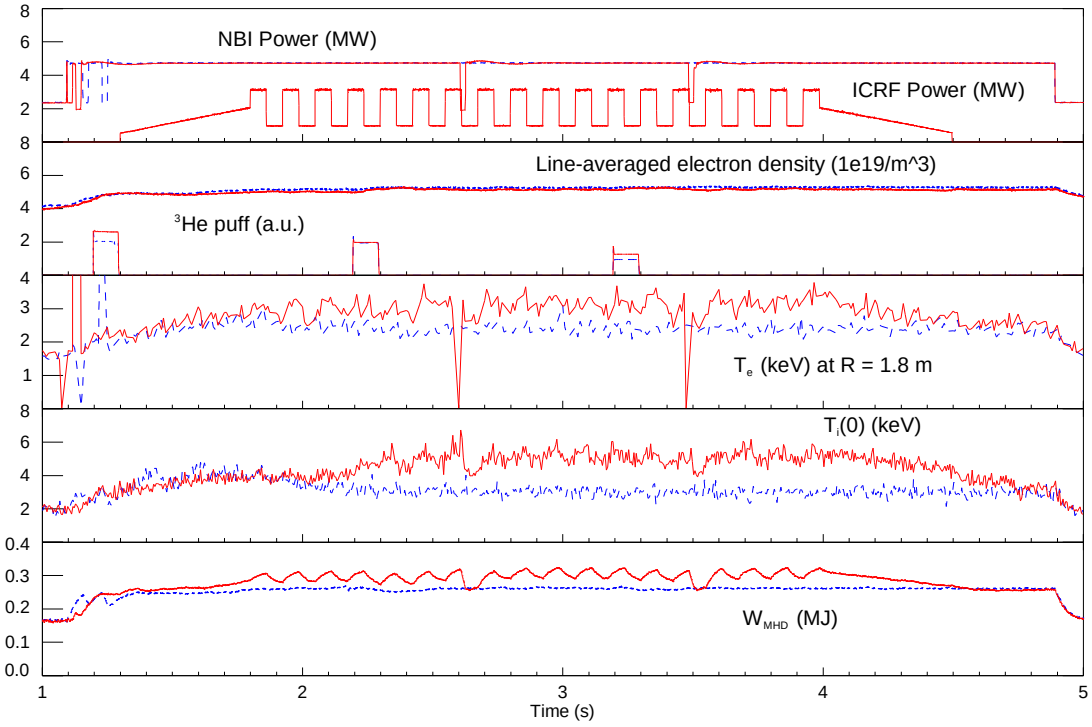


**FIGURE 2** Overview of plasma parameters for discharges 31555 (dashed, blue online) with NBI only and for discharge 31563 (solid, red online) with NBI and ICRF heating tuned to a central $^3$He resonance at $R_{res}$≈1.65 m (corresponding to x/a ≈ -0.1).

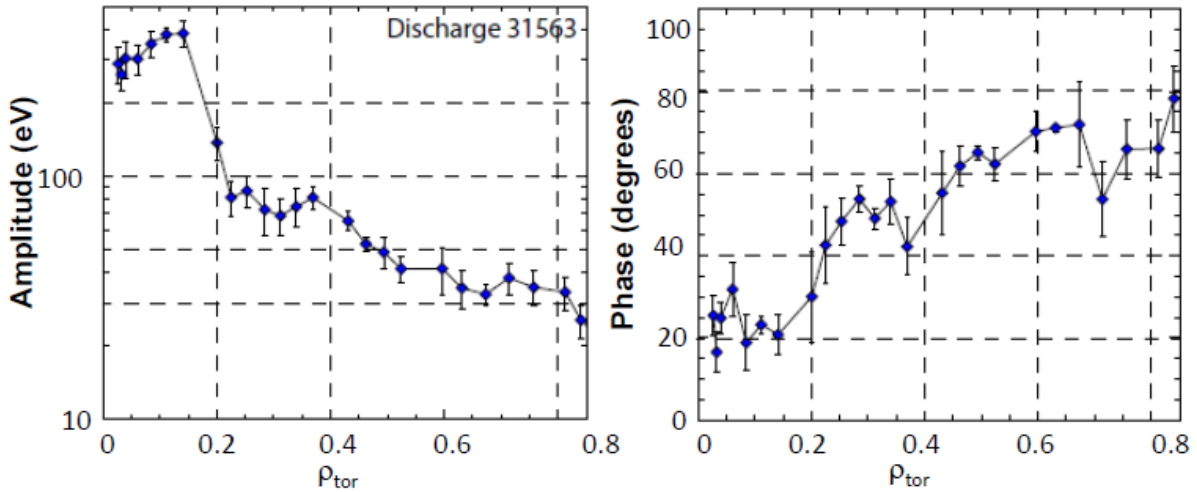


**FIGURE 3** Radial profile of the amplitude and phase of the ion temperature modulation with respect to the applied ICRF power modulation as deduced from CXSR measurements in discharge 31563 at a plasma current of 0.6 MA and a magnetic field of 3 T.

Significant differences are also observed in the 2D soft X-ray emission profiles in the poloidal plane, indicative of the impurity profile, as shown in Fig. 6. As we can see from Fig. 6, more peaked soft X-ray emission profiles were obtained when ICRF heating was applied. Furthermore, with an off-axis resonance in discharge 31562, a broader soft X-ray emission profile was obtained than with discharge 31563 with a central resonance. It is important to note that in spite of the peaked soft X-ray emission profiles, none of the discharged carried out in this series of experiments suffered from disruptions or radiative collapses.

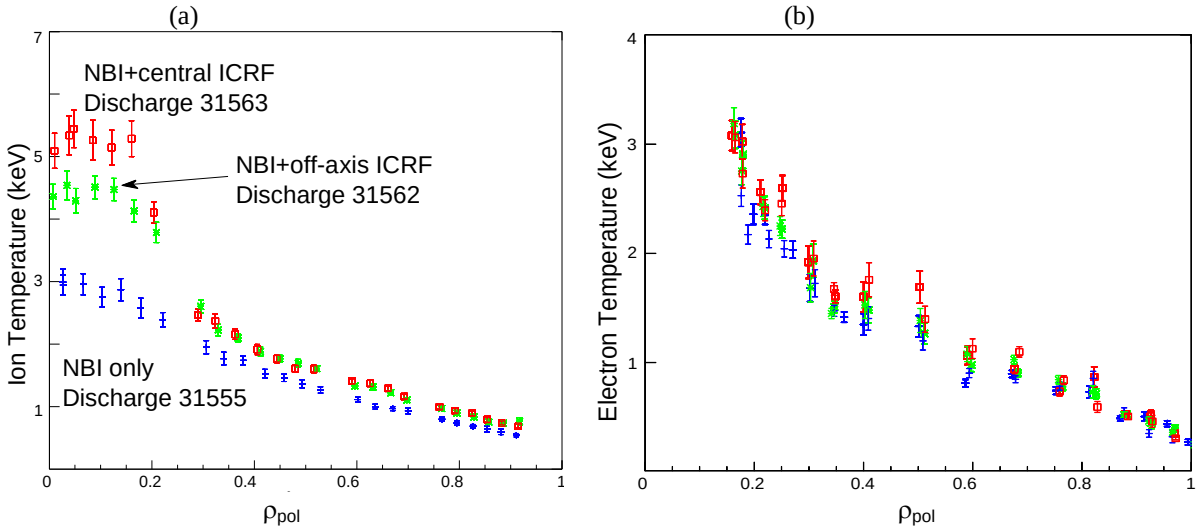


**FIGURE 4** Radial ion temperature profile as measured with CXSR and radial electron temperature profile as measured with Thomson scattering at t = 3 s for discharge 31555 with NBI only, discharge 31563 with NBI and central ICRF and discharge 31562 with NBI and off-axis ICRF as a function of $\rho_{pol} \approx r/a$ where r/a is the normalized plasma minor radius. The symbols in (b) are the same as in (a).

Important differences were also observed in the MHD activity. While discharge 31555 with NBI only showed regular sawteeth with a period of about 0.1s, with the application of $^3$He minority heating, the sawtooth activity disappeared and instead, fishbones appeared with a frequency in the range of 15-30 kHz. Given that fishbones typically appear in AUG plasmas when the fast ion beta increases above a critical value [19], the appearance of fishbones indicates an increase in the fast ion beta when ICRF power was applied.

The observed changes in the plasma rotation velocity profiles, the soft X-ray emission profiles and the MHD activity imply important changes in the plasma (transport) properties, which make the quantitative assessment of bulk ion heating efficiency due to ICRF waves rather challenging. For example, it is possible that the high central radiation losses due impurity accumulation could have caused transport changes due to high central radiation losses and contributed to the observed behaviour of the $T_i$ profiles and to the measured amplitude and phase of the $T_i$ modulation with respect to the applied ICRF modulation. Such effects need to be carefully taken into account in the assessment of the ion heating efficiency. There are also important plasma and ICRF physics questions that arise from the observations. For example, the key question regarding the observed impurity behaviour is why the impurity density peaks in spite of an increasing neoclassical screening by a peaked $T_i$ profile. From the ICRF point of view, the key issues are the overall similarity of the plasma behaviour with the central and off-axis resonance and the relative importance of electron and ion heating by ICRF in explaining the observed plasma performance. Apart from the central radiation losses, other candidates for the observed changes in the transport properties such as fast ion stabilisation of ion temperature gradient ITG turbulence [20,21] may need to be considered to understand the observations.

The analysis of the discharges with ICRF modelling has been initiated. In the simulations the measured plasma parameters are used, and the $^3$He concentration is assumed to be radially constant and equal to the $^3$He concentration as deduced from the CXSR measurements at mid-radius. Assuming a toroidal wave mode number N of 12, the full-wave code TORIC coupled with the Fokker-Planck solver SSFPQL [22] predicts a bulk ion heating fraction $\eta$ of 56-80% for discharge 31563, with a lower $\eta$ during the high power phase and a higher $\eta$ in the lower power phase of the ICRF power modulation. PION [23], assuming a single N of 12, gives similar results with $\eta$ varying between 70-

80%. Simulations have also been carried out with PION for the full N spectrum, which shows somewhat smaller η of 60-70% due to stronger competing direct electron damping. The power transfer profiles from ICRF waves to bulk ions and electrons as given by PION are shown in Figure 7a at t = 3.1 s towards the end of the phase with the maximum power of the ICRF power modulation for discharge 31563. The bulk ion and electron heating profiles are peaked around the resonance near the plasma center, where the power density reaches 0.4 and 0.8 MW/m$^3$ for ions and electrons, respectively. For comparison, the central bulk ion and electron heating power density due to NBI as given by TRANSP is about 1.0 and 0.35 MW/m$^3$, respectively. The simulated power deposition profiles are broadly consistent with the observed increase both in $T_i$ and $T_e$ with the application of ICRF heating in the plasma center. Furthermore, as shown in Fig. 7b, the total fast $^3$He ion pressure as given by PION is peaked around the resonance where the fast ion pressure reaches values up to about 10 kPa in discharge 31563. This corresponds to a fast $^3$He ion energy density of about 15 kJ/m$^3$, which is significantly smaller than the energy density of 60 kJ/m$^3$ of the NBI injected fast ions as given by TRANSP in the plasma center. Simulations with PION and TORIC + SSFPQL for discharge 31562 with an off-axis ICRF resonance are in progress.

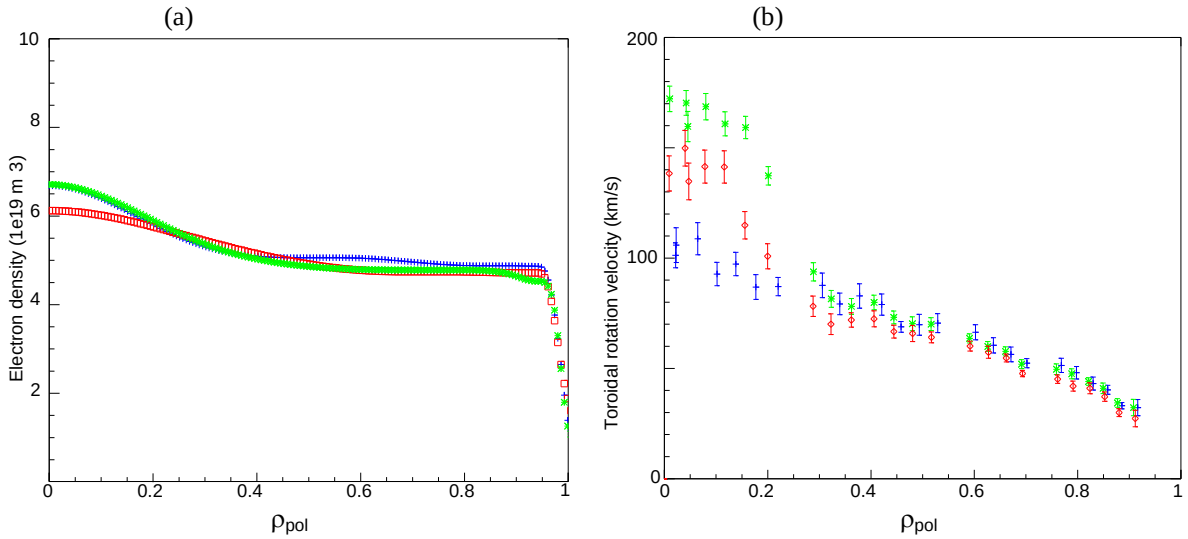


**FIGURE 5** (a) Electron density profile and (b) plasma toroidal rotation profile as measured with CXSR at t = 3 s for discharge 31555 with NBI only, discharge 31563 with NBI and on-axis ICRF, and discharge 31562 with NBI and off-axis ICRF as a function of $\rho_{pol} \approx r/a$. The symbols are as in Figure 4.

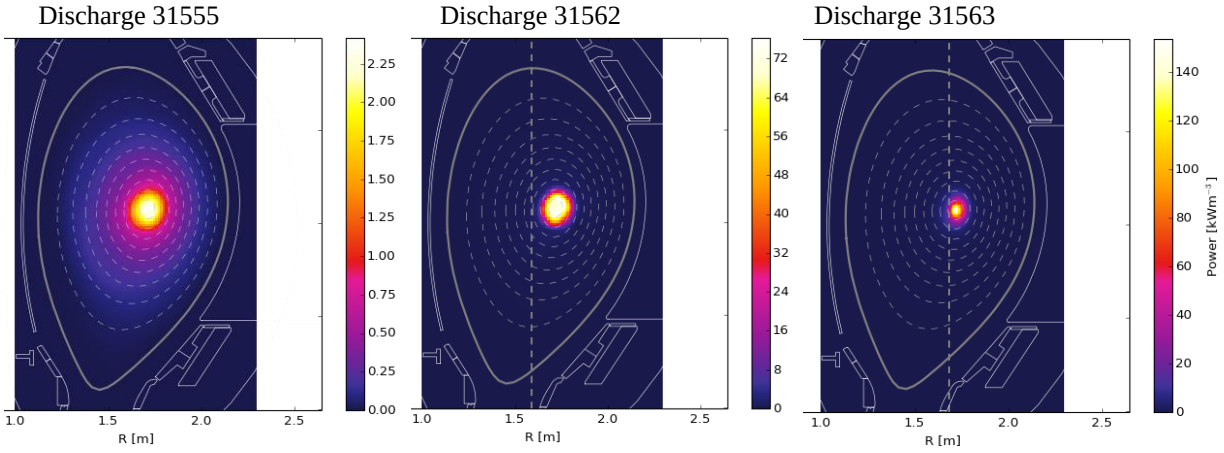


**FIGURE 6** Tomographic reconstruction of 2D soft X-ray emission profiles for discharges 31555, 31562 and 31563 with NBI only, with NBI and off-axis $^3$He minority heating, and with NBI and on-axis $^3$He minority heating, respectively. Note the large differences in the maximum emissivities as indicated by the color bars.

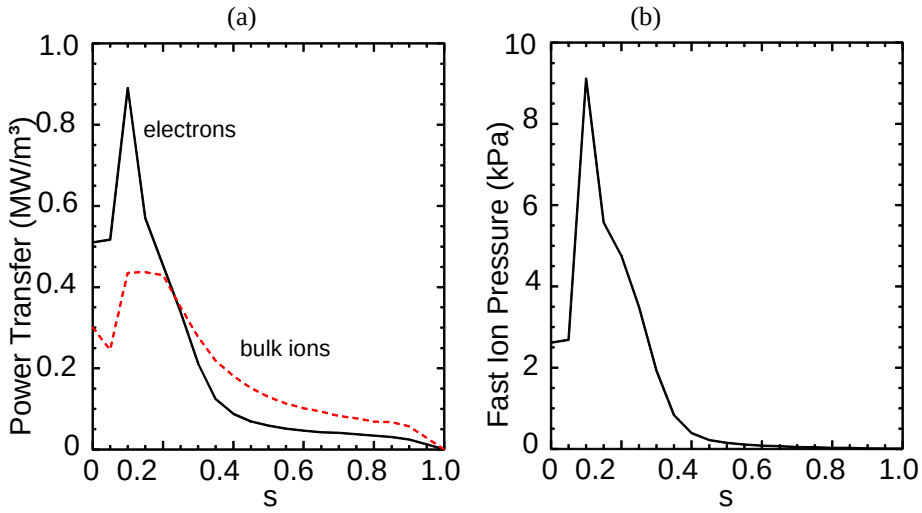


**FIGURE 7** Radial profile of (a) ICRF power transferred to bulk ions and electrons and (b) pressure of the ICRF-accelerated fast $^3$He ions as given by PION for discharge 31563 at t = 3.1 s. Here, s ≈ r/a is the square root of the normalized poloidal flux.

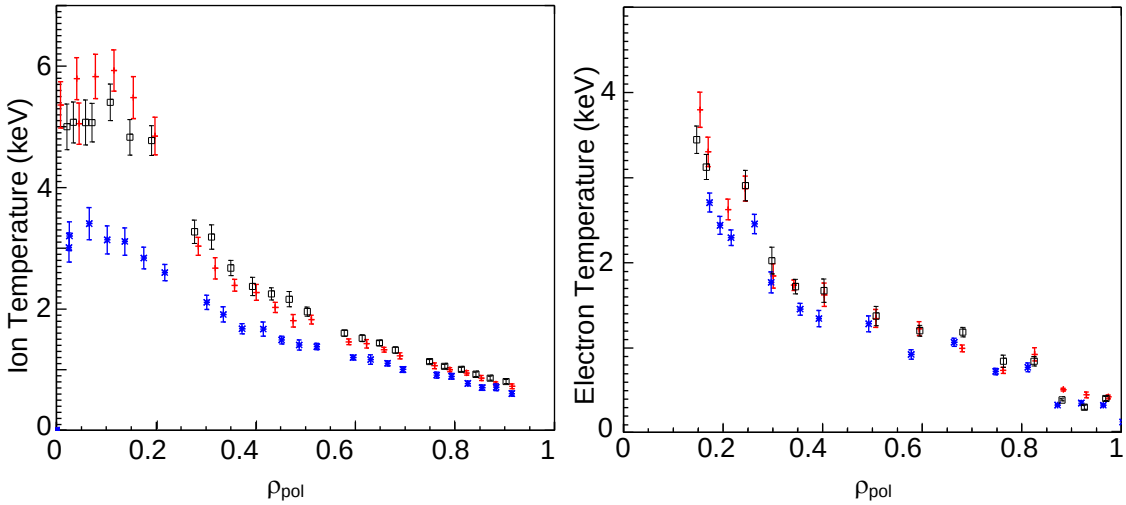


**FIGURE 8** Radial $T_i$ profile as measured by CXRS and radial $T_e$ profile as measured with Thomson scattering as a function of $\rho_{pol} \approx r/a$ at t = 3.1 s (+) and t = 3.4 s (□) for discharge 31585 and at t = 3.1 s for discharge 31587 (*). The $^3$He concentration was 6 and >10% in discharge 31585 and 31587, respectively.

Finally, we discuss the main results of discharges 31585 and 31587 where ICRF heating was also tuned to the central $^3$He resonance at $R_{res} \approx 1.65$ m (x/a ≈ -0.1). Discharge 31585 was carried out in order to compare the performance of $^3$He minority heating with NBI. Consequently, the high power phase of discharge 31585 was divided in two time windows with different ICRF and NBI wave forms. In the first time window ICRF power was modulated while keeping the NBI power constant. In the second time window, NBI power was modulated while keeping the ICRF power constant. The modulation amplitude was 2 MW, applied to the baseline heating of 0.9 MW and 4.5 MW of ICRF and NBI power, respectively. The $^3$He concentration was kept constant at about 6% throughout the heating phase. Figure 8 shows the resulting $T_i$ and $T_e$ profiles for NBI for the high power phase of NBI and ICRF power modulation cycle. As we can see from Fig. 8, very similar $T_i$ and $T_e$ profiles were obtained.

Figure 8 also shows the measured radial $T_i$ and $T_e$ profiles in discharge 31587. Discharge 31587 was prepared in the same way as discharge 31585 expect for the $^3$He puff which was increased with respect to discharge 31585. As a result, the $^3$He concentration as deduced from CXRS measurements at mid-radius increased from about 6 % in

discharge 31585 to above 10% in discharge 51687. As we can see from Fig. 8, the peaking of the $T_i$ profile was significantly reduced in discharge 31587 with respect to discharge 31585. As the $^3$He concentration was increased from 6 to above 10%, we expect that some of the ICRF power was mode converted to shorter-wavelength waves instead of being absorbed by $^3$He minority ions. In the present plasma conditions, the mode-converted shorter-wavelength waves are expected to give rise to off-axis power deposition mainly on electrons. Thus, the observed decrease in the ion temperature peaking with increasing $^3$He concentration appears consistent with the expected decrease in the central bulk ion heating by ICRF waves above the optimal $^3$He concentration for bulk ion heating.

## CONCLUSIONS

Heating with ICRF waves is a well-established method on present-day tokamaks and one of the heating systems foreseen for ITER. Moreover, it is the only scheme that can predominantly heat the bulk ions in ITER. The standard ITER ICRF scheme, $\omega = \omega(^3\text{He}) = 2\ \omega_T$, is compatible with bulk ion heating, as was demonstrated by experiments carried out in D-T plasmas on JET and TFTR in 1990's. This paper focused on recent experiments with bulk ion heating with $^3$He minority heating on AUG with ITER-relevant all-tungsten PFCs. An increase of 80% in the central $T_i$ from 3 to 5.5 keV was achieved when 3 MW of ICRF power tuned to the central $^3$He ion cyclotron resonance was added to 4.5 MW of deuterium NBI. The radial gradient of the $T_i$ profile reached locally values up to about 50 keV/m and its gradient scale length $R/L_{Ti}$ of about 20, which are unusually large for AUG plasmas. Given the observed impact on key plasma parameters such as $T_i$, $T_i/T_e$ ratio, toroidal rotation velocity and impurity profile, the scheme shows potential for performance optimization and further ITER physics studies on AUG.

## ACKNOWLEDGMENTS

This work has been carried out within the framework of the EUROfusion Consortium and has received funding from the Euratom research and training programme 2014-2018 under grant agreement No 633053. The views and opinions expressed herein do not necessarily reflect those of the European Commission.

## REFERENCES

1. V. Bergeaud, L.-G. Eriksson, D.F.H. Start, Nuclear Fusion 40(2000) 35.
2. R. Dumont and D. Zarzoso, Nuclear Fusion 53 (2013) 013002.
3. R. J. Dumont, Nuclear Fusion 49 (2009) 075033.
4. J.R. Wilson et al., Physical Review Letters 75 (1995) 842.
5. C.K. Phillips et al, Physics Plasmas 2 (1995) 2427.
6. M. Keilhacker et al., Nuclear Fusion 39 (1999) 209.
7. C. Gormezano et al., Physical Review Letters 80 (1998) 5544.
8. F.G. Rimini et al., Nuclear Fusion 39 (1999) 1591.
9. D.F.H. Start et al., Physical Review Letters 80 (1998) 4681.
10. D.F.H. Start et al., Nuclear Fusion 39 (1999) 321.
11. L.-G. Eriksson et al., Nuclear Fusion 39 (1999) 337.
12. G.A. Cottrell et al., Nuclear Fusion 39 (1999) 389.
13. P. Mantica et al., Physical Review Letters 102 (2009) 175002.
14. F. Ryter et al., Nuclear Fusion 51 (2011) 113016.
15. P.T. Bonoli et al., Fusion Science Technology 51 (2007) 401.
16. J.-M. Noterdaeme et al., 26th EPS Conf. on Contr. Fusion and Plasma Physics, Maastricht, 14 - 18 June 1999 ECA Vol. 23J (1999) 1561-1564.
17. J.-M. Noterdaeme et al., Radio-Frequency Power in Plasmas (13th Topical Conference RF Power in Plasmas, 1999, Annapolis, USA), AIP, New York, p. 92-99.
18. A. Kappatou, PhD thesis, Eindhoven University of Technology, the Netherlands (2014).
19. T. Kass et al., Nuclear Fusion 38 (1998) 807.
20. J. Citrin et al, Physical Review Letters, 111 (2013) 155001.
21. J. Garcia et al. Nuclear Fusion 55 (2015) 053007.
22. M. Brambilla and R. Bilato, Nuclear Fusion 49 (2009) 085004.
23. L.-G. Eriksson, T. Hellsten and U. Willén, Nuclear Fusion 33 (1993) 1037.